Effect of reduced dimensionality on the optical band gap of SrTiO3

Che-Hui Lee, Nikolas J. Podraza, Ye Zhu, Robert F. Berger, Shaoping Shen, Michelle Sestak, Robert W. Collins , Lena F. Kourkoutis, Julia A. Mundy, Huiqiong Wang, Qingyun Mao, Xiaoxing Xi, Leonard J. Brillson, Jeffrey B. Neaton, David A. Muller, and Darrell G. Schlom

Effect of reduced dimensionality on the optical band gap of SrTiO$_3$

Che-Hui Lee,[1,2] Nikolas J. Podraza,[3] Ye Zhu,[4] Robert F. Berger,[5] Shaoping Shen,[6]
Michelle Sestak,[3] Robert W. Collins,[3] Lena F. Kourkoutis,[4] Julia A. Mundy,[4]
Huiqiong Wang,[4] Qingyun Mao,[4] Xiaoxing Xi,[7] Leonard J. Brillson,[6] Jeffrey B. Neaton,[5]
David A. Muller,[4,8] and Darrell G. Schlom[1,8,a)]

[1]*Department of Materials Science and Engineering, Cornell University, Ithaca, New York 14853, USA*
[2]*Department of Materials Science and Engineering, Pennsylvania State University, University Park,
Pennsylvania 16802, USA*
[3]*Department of Physics and Astronomy, University of Toledo, Toledo, Ohio 43606, USA*
[4]*School of Applied and Engineering Physics, Cornell University, Ithaca, New York 14853, USA*
[5]*Molecular Foundry, Lawrence Berkeley National Laboratory, Berkeley, California 94720, USA*
[6]*Department of Electrical and Computer Engineering, Ohio State University, Columbus, Ohio 43210, USA*
[7]*Department of Physics, Temple University, Philadelphia, Pennsylvania 19122, USA*
[8]*Kavli Institute at Cornell for Nanoscale Science, Ithaca, New York 14853, USA*

The effect of dimensional confinement on the optical band gap of SrTiO$_3$ is investigated
by periodically introducing one extra SrO monolayer every n SrTiO$_3$ layers. The result is the
$n = 1$–5 and 10 members of the Sr$_{n+1}$Ti$_n$O$_{3n+1}$ Ruddlesden-Popper homologous series.
Spectroscopic ellipsometry, optical transmission, and cathodoluminescence measurements reveal
these Sr$_{n+1}$Ti$_n$O$_{3n+1}$ phases to have indirect optical band gaps at room temperature with values that
decrease monotonically with increasing n. First-principles calculations suggest that as n increases
and the TiO$_6$ octahedra become connected for increasing distances along the c-axis, the band edge
electronic states become less confined. This is responsible for the decrease in band gaps with
increasing n (for finite n) among Sr$_{n+1}$Ti$_n$O$_{3n+1}$ phases. © 2013 American Institute of Physics.
[http://dx.doi.org/10.1063/1.4798241]

With the increasing demand for sustainable green
energy, tuning the band gap of photovoltaic and photocatalytic materials has become of tremendous importance. For
example, the ability to tune the band gap of a photovoltaic
material is critical for developing high efficiency solar cells,
where the material is optimized to convert the solar spectrum
into electrical energy.[1] In addition, the width of the band gap
as well as the alignment of the conduction and valance bands
affects the ability of a material to split water photocatalytically.[2,3] Improved fundamental understanding of the effect
of systematic structural perturbations on the band gap and
related optical and electrical properties of common structures
can lead to the discovery of routes that tune electronic structure in desirable ways. Chemical substitution,[4–8] biaxial
strain,[9–12] and incorporation into a superlattice[13] have been
reported to effectively modify the optical band gap of semiconductors and functional oxides.

With its simple cubic structure and incredible variety of
properties, SrTiO$_3$—a compound with attributes including incipient ferroelectricity,[14] a large and tunable dielectric constant,[15] superconductivity,[16] robust photocatalysis,[17] and the
highest electron mobility of any oxide in bulk form[18]—is the
quintessential perovskite. In this study, SrTiO$_3$ is modified
through the periodic insertion of SrO planes to generate
a structurally related homologous series with chemical formula
(SrTiO$_3$)$_n$SrO (or equivalently Sr$_{n+1}$Ti$_n$O$_{3n+1}$, the Ruddlesden-Popper homologous series[19–21]) consisting of n monolayers of
perovskite SrTiO$_3$ alternating with a single additional layer of
rock-salt SrO along the c-axis [Fig. 1(a)]. As SrO layers are
inserted into SrTiO$_3$, its dimensionality is systematically modified from SrTiO$_3$, the $n = \infty$ member of this series in which the
corner-sharing TiO$_6$ octahedra are connected in three dimensions, to the two-dimensional version Sr$_2$TiO$_4$ ($n = 1$) in which
TiO$_6$ octahedra are connected as isolated sheets. The Sr$_3$Ti$_2$O$_7$
($n = 2$)[22] and Sr$_4$Ti$_3$O$_{10}$ ($n = 3$)[23] phases have been reported as
promising photocatalysts for water splitting.

Each unit cell of known Sr$_{n+1}$Ti$_n$O$_{3n+1}$ Ruddlesden-Popper phases contains two formula units and has tetragonal
symmetry with space group $I4/mmm$.[19,21] The growth of
phase-pure Sr$_{n+1}$Ti$_n$O$_{3n+1}$ samples in bulk form is limited by
thermodynamics to low n ($n \leq 3$) and $n = \infty$ (SrTiO$_3$).
Simulations[24–26] have found that Sr$_{n+1}$Ti$_n$O$_{3n+1}$ phases with
finite n become less stable with increasing n, and a limit of
stability at $n = 3$ has been predicted.[17] In agreement with these
calculations, conventional solid-state techniques have been
only able to make polycrystalline $n = 1$–3 samples.[19,21,27,28]
Attempts to make samples with higher, but finite, n result in
samples with disordered syntactic intergrowths.[29–31] These
intergrowths have prevented the investigation of the physical
properties of Sr$_{n+1}$Ti$_n$O$_{3n+1}$ phases with $3 < n < \infty$ on bulk
samples. To overcome this issue, Sr$_{n+1}$Ti$_n$O$_{3n+1}$ epitaxial
films have been synthesized by reactive molecular-beam
epitaxy[32–34] (MBE) and pulsed-laser deposition.[35–38] These
techniques have enabled the preparation of single crystalline
films of Sr$_{n+1}$Ti$_n$O$_{3n+1}$ phases with n up to 5 and investigation
of their dielectric constant as a function of direction.[32,34] How
the optical band gap changes with n has, however, not been
reported and is the subject of this letter.

In this study, we synthesize not only the first five
Sr$_{n+1}$Ti$_n$O$_{3n+1}$ phases but also the $n = 10$ and $n = \infty$
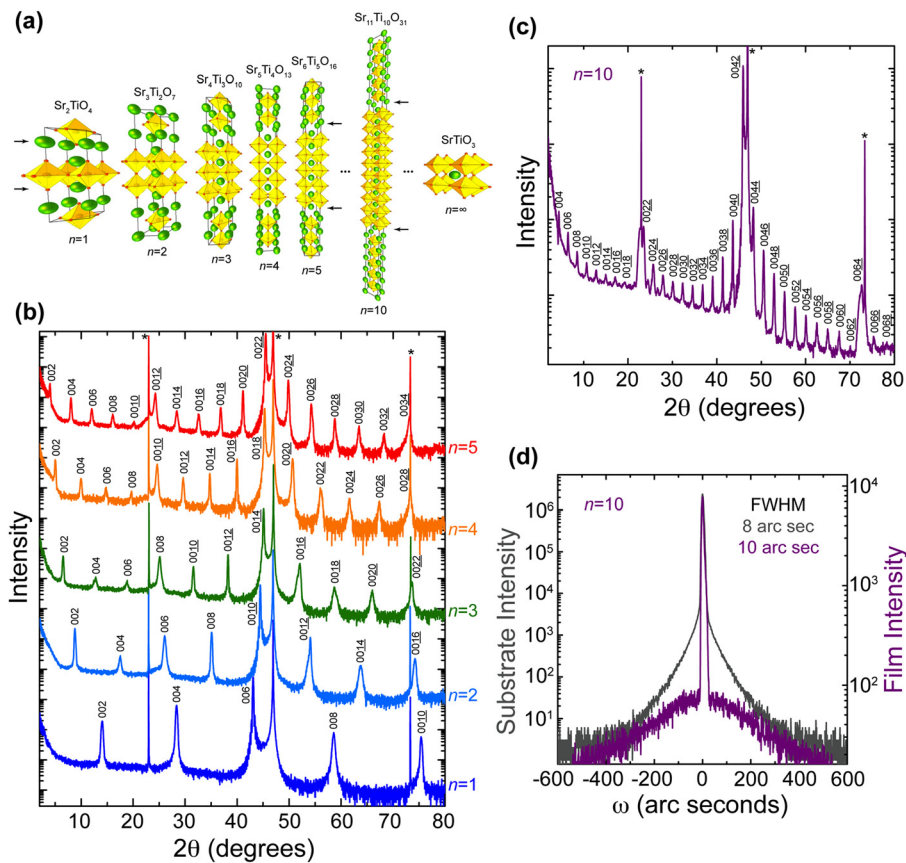
a)Electronic mail: schlom@cornell.edu.

FIG. 1. (a) Schematic of the crystal structure of a unit cell of the $n = 1-5$, 10, and ∞ members of the $Sr_{n+1}Ti_nO_{3n+1}$ Ruddlesden-Popper homologous series. The arrows indicate the additional layer of SrO. (b), (c) θ-2θ XRD scans of the epitaxial $Sr_{n+1}Ti_nO_{3n+1}$ films grown on (001) LSAT ($n = 1-5$, 10). Substrates peaks are labeled with a (*), and the plots are offset for clarity. (d) Superimposed XRD rocking curves of the $n = 10$ film (0042 peak) and underlying LSAT substrate (002 peak).

($SrTiO_3$) members (experimental details of film growth are provided in S1 of Ref. 39). In contrast to prior studies where the substrate was (001) $SrTiO_3$,[32,33] in this work, we used (001) $(LaAlO_3)_{0.29}(SrAl_{0.5}Ta_{0.5}O_3)_{0.71}$ (LSAT) substrates because its larger band gap[40] does not interfere with our optical measurements of the band gaps of the $Sr_{n+1}Ti_nO_{3n+1}$ films grown upon it. These artificial superlattices have the largest unit cells of any Ruddlesden-Popper phases ever made. The complex dielectric function spectra and optical band gaps of the complete series are measured by spectroscopic ellipsometry (SE) and compared to first-principles density functional theory. Band gap values are confirmed by the analysis of optical transmission and cathodoluminescence measurements.

The structural perfection of the epitaxial $Sr_{n+1}Ti_nO_{3n+1}$ films with $n = 1-5$, 10 was examined by four-circle XRD. Figures 1(b) and 1(c) show the θ-2θ scans of 500 Å thick $n = 1-5$, 10 films. Each sample shows all peaks corresponding to phase-pure $Sr_{n+1}Ti_nO_{3n+1}$ ($n = 1-5$, 10). Rocking curves confirmed the high structural perfection of the films (the $n = 10$ phase is shown in Fig. 1(d), and the $n = 1-5$ phases are shown in Fig. S2 of Ref. 39); the full width at half maximum (FWHM) of these films is <13 arc sec ($< 0.004°$), comparable to the rocking curve FWHM of the 002 peak of the LSAT substrates. The c-axis lattice constants of the entire series determined by Nelson-Riley analysis[41] are 12.60 ± 0.01 Å, 20.41 ± 0.02 Å, 28.24 ± 0.04 Å, 35.87 ± 0.02 Å, 43.81 ± 0.02 Å, and 82.95 ± 0.02 Å for the $n = 1-5$, 10 phases, respectively.

Figure 2 shows annular-dark-field scanning transmission electron microscope (STEM) images taken from the $n = 1, 3$, 5, and 10 films, using a 200 kV FEI Tecnai F20 SuperTWIN

STEM. Titanium columns show lower intensity than strontium columns in annular-dark-field STEM images. The structure of the films is in agreement with the models for $n = 1, 3$, 5, and 10 $Sr_{n+1}Ti_nO_{3n+1}$ unit cells (on the left side). Defects such as vertically running SrO double layers, however, remain and cause the images to appear patchy especially for the $n = 10$ film, which is the most thermodynamically unfavourable of this series.

The optical band gap of the entire $Sr_{n+1}Ti_nO_{3n+1}$ ($n = 1-5$, 10, ∞) series on LSAT substrates was determined by *ex situ* spectroscopic ellipsometry and optical transmission measurements at room temperature. Room temperature ellipsometric spectra (in Δ and ψ) were collected at two angles of incidence, $\Theta_i = 55°$ and $70°$, using a variable-angle rotating-compensator multichannel spectroscopic ellipsometer[42,43] over a spectral range from 0.75 to 6.5 eV. Unpolarized optical transmission spectra were collected at normal incidence over a spectral range from 1.5 to 5.0 eV. The complex dielectric function ($\varepsilon = \varepsilon_1 + i\varepsilon_2$) and microstructural parameters (bulk layer thickness and surface roughness) were extracted using a least squares regression analysis and an unweighted error function[44] to fit the experimental ellipsometric spectra to a scattering matrix based optical model of coherent multiple reflections propagating in the semi-infinite LSAT substrate/bulk $Sr_{n+1}Ti_nO_{3n+1}$ film/surface roughness/air ambient structure. Free parameters in the model correspond to the bulk and surface roughnesses of the $Sr_{n+1}Ti_nO_{3n+1}$ film and a parameterization of ε for the $Sr_{n+1}Ti_nO_{3n+1}$. The parameterization of ε for each $Sr_{n+1}Ti_nO_{3n+1}$ film was represented by five Tauc-Lorentz oscillators[45,46] sharing a common absorption onset and a constant additive term to ε_1, represented by ε_∞. The optical properties of the surface roughness layer were
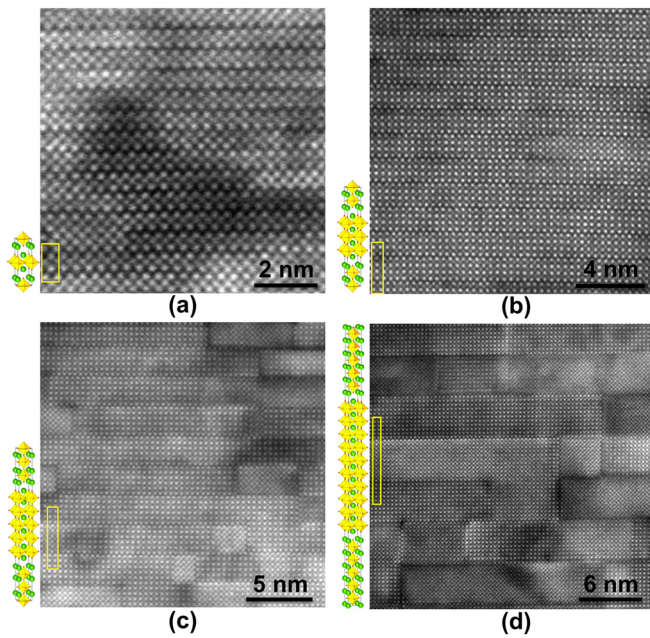
FIG. 2. Annular-dark-field STEM images of the epitaxial Ruddlesden-Popper films: (a) $n = 1$ (Sr$_2$TiO$_4$), (b) $n = 3$ (Sr$_4$Ti$_3$O$_{10}$), (c) $n = 5$ (Sr$_6$Ti$_5$O$_{16}$), (d) $n = 10$ (Sr$_{11}$Ti$_{10}$O$_{31}$) film grown on LSAT. Unit cell models of the corresponding Ruddlesden-Popper phases are placed on the left side of the images, which correspond to the yellow-rectangle highlighted part in the images.

FIG. 3. (a) Comparison of the complex dielectric function spectra ($\varepsilon = \varepsilon_1 + i\varepsilon_2$) obtained by numerical inversion for Sr$_{n+1}$Ti$_n$O$_{3n+1}$ ($n = 1$–5, 10, ∞) films on LSAT substrates. (b) Plots of $\alpha^{1/2}$ and α^2 as functions of photon energy for Sr$_2$TiO$_4$ ($n = 1$) prepared on LSAT. The indirect band gap is found by fitting $\alpha^{1/2}$ to a line and noting where $\alpha^{1/2} = 0$. The direct gap is found by fitting α^2 to a line and noting where $\alpha^2 = 0$.

represented by a Bruggeman effective medium approximation[47] consisting of a 0.5 bulk film/0.5 void mixture.

An LSAT substrate was characterized using the same process to determine its structure and reference optical properties. The LSAT substrates used in this study had approximately 16 Å of surface roughness determined in this manner, while that of the films ranged from 23 to 53 Å with decreasing n. The surface roughness layer thickness measured optically on the LSAT substrate may be due to a combination of roughness and contaminants on the surface, as the inclusion of an interfacial layer between LSAT and the Sr$_{n+1}$Ti$_n$O$_{3n+1}$ film in modelling the spectra of the substrate/film samples did not significantly affect the fit. As the surface roughness of the films was sufficiently low so that variations in the void fraction and surface roughness become correlated, the void and bulk material fractions were fixed at 0.5 in this layer.

After bulk film and surface roughnesses were obtained from the parameterized model, numerical inversion was used to extract ε as a function of photon energy directly from the experimental ellipsometric spectra. Similarly, these structural parameters, a scattering matrix model using coherent interference effects and incoherent multiple reflections within the finite-thickness LSAT substrate, and the measured thickness of the LSAT substrates, which ranged from $\sim$0.6–1.0 mm with variations due to polishing of the back side of the sample, were used to extract the absorption coefficient, α, as a function of photon energy directly from the optical transmission spectra. The minimum values of ε_2 obtained for these samples ranged from $\sim$0.02 to 0.05.

Figure 3(a) shows a comparison of ε across the Sr$_{n+1}$Ti$_n$O$_{3n+1}$ ($n = 1$–5, 10, ∞) series. By comparing the sets of spectra, all films seem to share critical point features at comparable energies above $\sim$4.0 eV. Below 4.0 eV in the
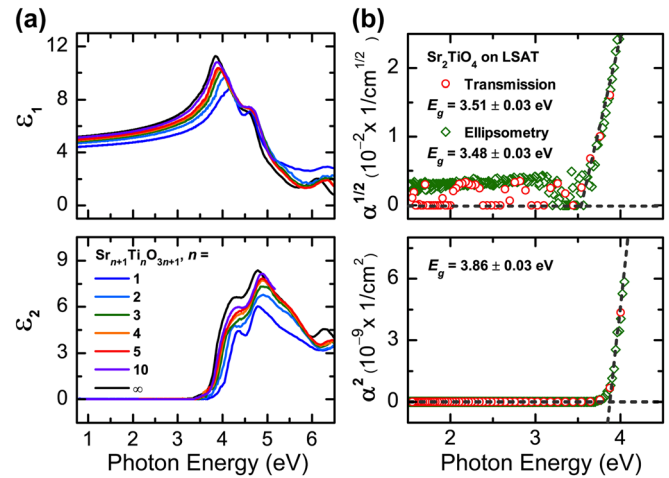
ε_2 spectrum, however, it is observed that the films exhibit increasing low energy absorption with increasing n, and the small critical point feature in the vicinity of $\sim$3.75 eV present for SrTiO$_3$ is damped for lower n.

ε obtained from numerical inversion of the ellipsometric spectra is converted to the absorption coefficient, α, as a function of photon energy. $\alpha^{1/2}$ and α^2 obtained from spectroscopic ellipsometry and optical transmission measurements are then plotted as functions of photon energy [Fig. 3(b)] and extrapolated using a linear relationship to $\alpha^{1/2}$ (α^2) = 0 to identify the indirect (direct) band gap as has been previously used to identify the band gap of SrTiO$_3$.[48,49] From the plot of $\alpha^{1/2}$ as a function of photon energy, it is observed that there is a line with a high slope and an intercept $\sim$3.5 eV.

There is significant noise and a loss of sensitivity below this intercept in the data collected from ellipsometry. Artifacts in the optical transmission spectra potentially arise from sampling different spots on the surface by each optical technique while analysing using the same optical model and structural parameters or potentially from changes in the LSAT substrate arising from heating during film deposition. Thus, the band gap values reported from this analysis may not be absolute, as a second line attributed to phonons with lower slope extending to lower photon energies was not able to be adequately quantified. The values reported here extrapolate the intercept of $\alpha^{1/2}$ = 0 using a range from $2000 < \alpha < 40\,000$ 1/cm, using a span of α intermediate to that adopted for SrTiO$_3$ in Refs. 48 and 49. At the very least, these values represent the location of the absorption edge as a function of n obtained in a self-consistent approach. All results from spectroscopic ellipsometry (Fig. 4) follow similar behaviour and the band gap determined from $\alpha^{1/2} = 0$ decreases monotonically from 3.48 ± 0.025 eV ($n = 1$) to 3.15 ± 0.025 eV ($n = \infty$) with increasing n. Results from optical transmittance (Fig. 4) also exhibit a decrease in band gap from 3.51 ± 0.03 eV ($n = 1$) to 3.30 ± 0.05 eV ($n = 10$). A similar decrease is observed in the direct gap by extrapolation of $\alpha^2 = 0$ obtained from spectroscopic ellipsometry and transmittance (Fig. 4).
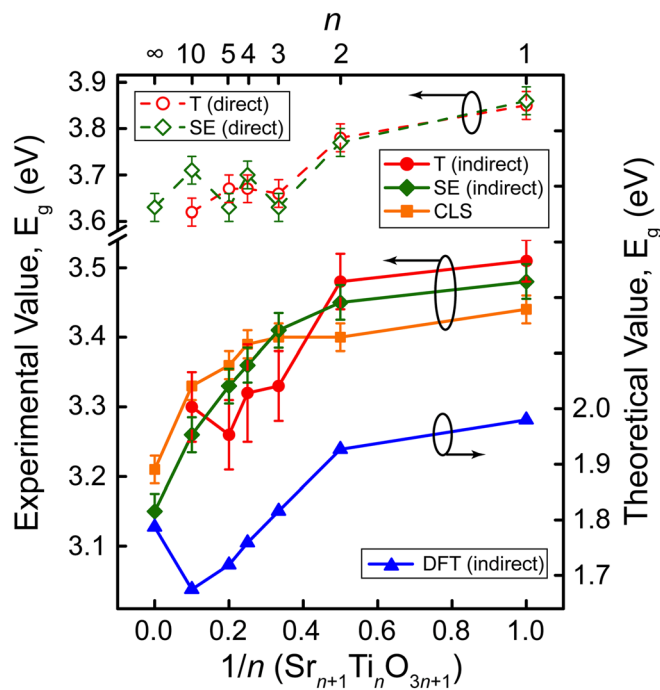
FIG. 4. Band gaps as a function of n in $Sr_{n+1}Ti_nO_{3n+1}$ ($n = 1–5$, 10, ∞) films. Indirect band gap values determined experimentally by transmission (T, solid circles, full line), SE (solid diamonds, full line), CLS (solid squares, full line), and by DFT-LDA calculations (DFT, solid triangles, full line) are shown. Direct band gap values determined by transmission (T, open circles, dashed line) and SE (open diamonds, dashed line) are shown as well.

The band gaps determined by cathodoluminescence spectroscopy (CLS)[50] on the same sample set are in agreement with the values obtained from ellipsometry and optical transmission spectra (Fig. 4). Extracting the CLS band gap required systematically deconvolving the band edge emission from a large substrate defect contribution. The LSAT substrate contributed the dominant signal to the spectrum. In order to establish a precise band gap value, we subtracted this defect emission from the total spectrum to establish a new baseline that yielded the band edge emission peak. The experimental band gaps of the $Sr_{n+1}Ti_nO_{3n+1}$ ($n = 1–5$, 10) phases fall between the high band gap SrO ($n = 0$) and SrTiO$_3$ ($n = \infty$) end members of the series[48,49,51] (experimental details of CLS measurements are provided in S3 of Ref. 39).

Our optical band gap results are in qualitative agreement with the only prior reports of the optical band gaps of members of this series.[28,52] For $n = 1$, the optical band gap has been reported to be 3.4 eV and 3.9 eV.[28,52] For $n = 2$, the only report is 3.1 eV, which the authors found to be the same as their SrTiO$_3$ control samples.[28] This disagrees with our results where we find $n = 2$ to have an optical band gap about 0.2 eV higher than $n = \infty$ and could be due to higher n intergrowths in the polycrystalline $n = 2$ samples previously studied.[28] Our work fills the gap between $n = 2$ and $n = \infty$ members and provides high quality data on $Sr_{n+1}Ti_nO_{3n+1}$ phases inaccessible to bulk synthesis techniques (a table of experimental band gap values obtained in this work is provided in S5 of Ref. 39).

In addition to the measured band gaps (left axis), Fig. 4 also shows the computed band gaps (right axis) of these

$Sr_{n+1}Ti_nO_{3n+1}$ phases from first-principles density functional theory (DFT) calculations within the local density approximation (LDA). Kohn-Sham indirect band gaps were calculated as the difference between the conduction band minimum (CBM, Γ point) and valence band maximum (VBM, R point for SrTiO$_3$ and X point for finite n). Separate axes are used because DFT-LDA calculations significantly underestimate band gaps, a result of their neglecting many-electron interactions.[53,54] Nonetheless, they can capture qualitative trends,[55–57] as seen in the analogous dependence of the measured and calculated band gaps in Fig. 4 on n for finite n. The decrease in band gaps with increasing finite n can be attributed to a reduction in confinement energy as the states bracketing the band gap (nonbonding combinations of Ti 3d orbitals in the case of the CBM and antibonding O 2p orbitals in the case of the VBM) reside in regions of connected octahedra that are increasingly extended in a third dimension.

In notable contrast to experiment, however, computed band gaps for $3 < n < \infty$ are smaller than that of SrTiO$_3$ ($n = \infty$). It is not altogether surprising that this discontinuity is seen in theory, but not experiment as the two band gaps are obtained in fundamentally different ways. Our Kohn-Sham band gaps are simply differences between CBM and VBM energies. The discontinuity at $n = \infty$ arises from a change in the spatial makeup of the CBM—in short, because finite n structures have SrO bilayers while $n = \infty$ does not. CBM states for large finite n consist mainly of Ti 3d orbitals confined to two-dimensional layers on either side of the SrO bilayers, while SrTiO$_3$ CBM states are fully three-dimensional combinations of Ti 3d orbitals (further explanation of the band gap changes due to dimensionality is provided in S4 of Ref. 39). Experiments, however, obtain the band gap from an extrapolation of optical spectra near the absorption edge onset. As n gets large, the contribution of SrO bilayers to the density of states vanishes, leading the optical behaviour (and the properties extracted from it, including band gap) to approach that of $n = \infty$. For a quantitative comparison of theory to experiment, one must calculate the full optical spectra of these compounds (including electron-hole interactions) and extract the band gaps as they are taken in experiment. Such analysis will be explored in future theoretical work.

[1] D. M. Chapin, C. S. Fuller, and G. L. Pearson, J. Appl. Phys. **25**, 676 (1954).
[2] A. Fujishima and K. Honda, Nature **238**, 37 (1972).
[3] A. Kudo and Y. Miseki, Chem. Soc. Rev. **38**, 253 (2009).

[4]H. Kroemer, RCA Rev. **18**, 332 (1957).

[5]F. Capasso, Science **235**, 172 (1987).

[6]R. F. Davis, Proc. IEEE **79**, 702 (1991).

[7]J. W. Bennett, I. Grinberg, and A. M. Rappe, J. Am. Chem. Soc. **130**, 17409 (2008).

[8]W. S. Choi, M. F. Chisholm, D. J. Singh, T. Choi, G. E. Jellison, Jr., and H.-N. Lee, Nat. Commun. **3**, 689 (2012).

[9]W. Shockley and J. Bardeen, Phys. Rev. **77**, 407 (1950).

[10]C. S. Smith, Phys. Rev. **94**, 42 (1954).

[11]M. M. Roberts, L. J. Klein, D. E. Savage, K. A. Slinker, M. Friesen, G. Celler, M. A. Eriksson, and M. G. Lagally, Nature Mater. **5**, 388 (2006).

[12]M. S. Leite, E. C. Warmann, G. M. Kimball, S. P. Burgos, D. M. Callahan, and H. A. Atwater, Adv. Mater. **23**, 3801 (2011).

[13]M. Helm, W. Hilber, T. Fromherz, F. M. Peeters, K. Alavi, and R. N. Pathak, Phys. Rev. B **48**, 1601 (1993).

[14]K. A. Müller and H. Burkard, Phys. Rev. B **19**, 3593 (1979).

[15]E. Hegenbarth, Phys. Status Solidi **6**, 333 (1964).

[16]J. F. Schooley, W. R. Hosler, and M. L. Cohen, Phys. Rev. Lett. **12**, 474 (1964).

[17]M. S. Wrighton, A. B. Ellis, P. T. Wolczanski, D. L. Morse, H. B. Abrahamson, and D. S. Ginley, J. Am. Chem. Soc. **98**, 2774 (1976).

[18]O. N. Tufte and P. W. Chapman, Phys. Rev. **155**, 796 (1967).

[19]D. Balz and K. Plieth, Z. Elektrochem. **59**, 545 (1955).

[20]S. N. Ruddlesden and P. Popper, Acta Crystallogr. **10**, 538 (1957).

[21]S. N. Ruddlesden and P. Popper, Acta Crystallogr. **11**, 54 (1958).

[22]H. Jeong, T. Kim, D. Kim, and K. Kim, Int. J. Hydrogen Energy **31**, 1142 (2006).

[23]Y. G. Ko and W. Y. Lee, Catal. Lett. **83**, 157 (2002).

[24]K. R. Udayakumar and A. N. Cormack, J. Am. Ceram. Soc. **71**, C469 (1988).

[25]M. A. McCoy, R. W. Grimes, and W. E. Lee, Philos. Mag. A **75**, 833 (1997).

[26]C. Noguera, Philos. Mag. Lett. **80**, 173 (2000).

[27]G. J. McCarthy, W. B. White, and R. Roy, J. Am. Ceram. Soc. **52**, 463 (1969).

[28]H. W. Eng, P. W. Barnes, B. M. Auer, and P. M. Woodward, J. Solid State Chem. **175**, 94 (2003).

[29]P. L. Wise, I. M. Reaney, W. E. Lee, T. J. Price, D. M. Iddles, and D. S. Cannell, J. Eur. Ceram. Soc. **21**, 2629 (2001).

[30]K. Hawkins and T. J. White, Philos. Trans. R. Soc. London, Ser. A **336**, 541 (1991).

[31]R. J. D. Tilley, J. Solid State Chem. **21**, 293 (1977).

[32]J. H. Haeni, C. D. Theis, D. G. Schlom, W. Tian, X. Q. Pan, H. Chang, I. Takeuchi, and X.-D. Xiang, Appl. Phys. Lett. **78**, 3292 (2001).

[33]W. Tian, X. Q. Pan, J. H. Haeni, and D. G. Schlom, J. Mater. Res. **16**, 2013 (2001).

[34]N. D. Orloff, W. Tian, C. J. Fennie, C.-H. Lee, D. Gu, J. Mateu, X. X. Xi, K. M. Rabe, D. G. Schlom, I. Takeuchi, and J. C. Booth, Appl. Phys. Lett. **94**, 042908 (2009).

[35]Y. Iwazaki, T. Suzuki, S. Sekiguchi, and M. Fujimoto, Jpn. J. Appl. Phys., Part 2 **39**, L303 (2000).

[36]K. Shibuya, S. Mi, C.-L. Jia, P. Meuffels, and R. Dittmann, Appl. Phys. Lett. **92**, 241918 (2008).

[37]M. Okude, A. Ohtomo, T. Kita, and M. Kawasaki, Appl. Phys. Express **1**, 081201 (2008).

[38]M. Okude, M. Saito, S. Tsukimoto, A. Ohtomo, M. Tsukada, M. Kawasaki, Y. Ikuhara, and Z. Wang, Nat. Commun. **1**, 106 (2010).

[39]See supplementary material at http://dx.doi.org/10.1063/1.4798241 for additional details on film growth, XRD rocking curves of the $Sr_{n+1}Ti_nO_{3n+1}$ ($n = 1–5$) samples, experimental details of the cathodoluminescence spectroscopy measurements, further explanation for the band gap changes due to dimensionality, and a table of experimental band gap values.

[40]B. J. Gibbons and S. Trolier-McKinstry, IEEE Trans. Appl. Supercond. **7**, 2177 (1997).

[41]J. B. Nelson and D. P. Riley, Proc. Phys. Soc. London **57**, 160 (1945).

[42]J. Lee, P. I. Rovira, I. An, and R. W. Collins, Rev. Sci. Instrum. **69**, 1800 (1998).

[43]B. D. Johs, J. A. Woollam, C. M. Herzinger, J. N. Hilfiker, R. A. Synowicki, and C. L. Bungay, Proc. SPIE **CR72**, 29 (1999).

[44]Y. Cong, I. An, K. Vedam, and R. W. Collins, Appl. Opt. **30**, 2692 (1991).

[45]G. E. Jellison and F. A. Modine, Appl. Phys. Lett. **69**, 371 (1996).

[46]G. E. Jellison and F. A. Modine, Appl. Phys. Lett. **69**, 2137 (1996).

[47]H. Fujiwara, J. Koh, P. I. Rovira, and R. W. Collins, Phys. Rev. B **61**, 10832 (2000).

[48]S. Zollner, A. A. Demkov, R. Liu, P. L. Fejes, R. B. Gregory, P. Alluri, J. A. Curless, Z. Yu, J. Ramdani, R. Droopad, T. E. Tiwald, J. N. Hilfiker, and J. A. Woollam, J. Vac. Sci. Technol. B **18**, 2242 (2000).

[49]K. van Benthem, C. Elsässer, and R. H. French, J. Appl. Phys. **90**, 6156 (2001).

[50]L. J. Brillson, J. Vac. Sci. Technol. B **19**, 1762 (2001).

[51]*Landolt-Börnstein: Numerical Data and Functional Relationships in Science and Technology*, New Series, Group III, edited by O. Madelung, M. Schulz, and H. Weiss, (Springer, Berlin, 1982), Vol. 17b, pp. 22 and 27.

[52]J. Matsuno, Y. Okimoto, M. Kawasaki, and Y. Tokura, Phys. Rev. Lett. **95**, 176404 (2005).

[53]G. Onida, L. Reining, and A. Rubio, Rev. Mod. Phys. **74**, 601 (2002).

[54]S. Kümmel and L. Kronik, Rev. Mod. Phys. **80**, 3 (2008).

[55]X. Zhu, S. Fahy, and S. G. Louie, Phys. Rev. B **39**, 7840 (1989).

[56]X. Zhao, C. M. Wei, L. Yang, and M. Y. Chou, Phys. Rev. Lett. **92**, 236805 (2004).

[57]R. F. Berger, C. J. Fennie, and J. B. Neaton, Phys. Rev. Lett. **107**, 146804 (2011).